# Towards application of LiDAR sensor to traffic detection: an investigation of its built-in features and installation techniques

**Junxuan Zhao**
Research Assistant
Department of Civil, Environmental, and Construction Engineering
Texas Tech University, Lubbock, TX 79409
Email: junxuan.zhao@ttu.edu

**Hao Xu**
Associate Professor
Department of Civil and Environmental Engineering
University of Nevada Reno, Reno, NV 89557
Email: haox@unr.edu

**Yuan Tian**
Research Assistant
Department of Civil and Environmental Engineering
University of Nevada Reno, Reno, NV 89557
Email: yuantian@nevada.unr.edu

**Hongchao Liu (corresponding author)**
Professor
Department of Civil, Environmental, and Construction Engineering
Texas Tech University, Lubbock, TX 79409
Email: hongchao.liu@ttu.edu

# Towards application of LiDAR sensor to traffic detection: an investigation of its built-in features and installation techniques


## ABSTRACT

In transportation, LiDAR sensors have been primarily used in surveying and autonomous driving as a major onboard sensing device to detect field objects. Recently, with reduced price and increased demand from real-time and trajectory-level traffic detection, LiDAR technology sees great potential for becoming a mainstream means of infrastructure-based traffic detection other than only being used onboard. In addition to its many advanced features, LiDAR is much less impacted by illumination conditions compared to video sensors and significant in data processing speed, which makes it ideal for real-time traffic detection. The research team has conducted a wealth of studies to investigate the feasibility of installing LiDAR sensors at the roadside to obtain trajectories of automobiles and pedestrians at a frequency of 10Hz. While our findings on how to process roadside LiDAR data have been presented in other literatures, this paper reveals our findings on another important issue regarding roadside LiDAR application - installation strategies to achieve the best performance. The authors first developed a theoretical approach based on the analysis of the built-in features of the applied LiDAR sensors and followed the results to install the sensors in our testbed. Then, experimental studies were conducted onsite and examined the theoretical results accordingly. As a result, a technical guidance for proper installation of LiDAR sensors at the roadside for the best real-time and trajectory-level traffic detection was produced. This study helps researchers and practitioners in better preparing for future deployment of roadside LiDAR sensors as part of the connected vehicles and infrastructures.


*Keywords*: roadside LiDAR; installation; height; inclination; detection range.

## 1. INTRODUCTION

Laser is one of the major inventions of the twentieth century. With recent advancement in electronic and communication technologies, laser sensors with smaller size and higher precision have been developed. An important application of the laser is Light Detection and Ranging (LiDAR), which measures distance to a target by illuminating the target with pulsed laser light and analyzing the reflected pulses. This is a typical non-contact active measurement technique that provides digitalized 3-dimensional (3D) of a target based on the differences in laser return times and wavelengths. High-accuracy point clouds data can be collected quickly, stably, and reliably during both daytime and nighttime (Csanyi & Toth, 2007). In the past decade, LiDAR has been widely used in remote sensing. For example, airborne LiDAR sensors are used to measure vertical structure, bulk density, base and peak heights of forest canopy in forest industry (Ahmed, Franklin, Wulder, & White, 2016). Bathymetric LiDAR is a technique to capture geospatial data of coastlines and shallow waters as well as creating hydrographic data (Mandlburger, Hauer, Wieser, & Pfeifer, 2015). Terrestrial LiDAR sensors are the top choice for archeological survey, landslide monitoring, coastal erosion analysis, etc. (Mahmud, Mariethoz, Treble, & Baker, 2015; Kromer, Lato, Hutchinson, Gauthier, & Edwards, 2017; Westoby et al., 2018).

LiDAR sensors have great potential to become a major traffic detection means and many traffic sensors currently deployed may be replaced by LiDAR sensor as its price continues to drop. As a commonly used traffic detection means, inductive loops cannot capture vehicle trajectories and maintenance is costly and labor-intensive (Klein, Mills, Gibson, & Klein, 2006). Video camera is another popular sensor that uses image information for traffic detection, however, illumination and weather conditions have significant impact on video quality and considerable computation time are needed for processing image data, especially for 3D video images (Wen, Shao, Fang, & Xue, 2015; Bautista, Dy, Mañalac, Orbe, & Cordel, 2016; Qu, Jiang, & Guo, 2016). Radar works in a similar way as LiDAR, except that it uses radio waves rather than lasers to determine the velocity and range of objects. It measures speed based on the Doppler effect, commonly used radar sensors in traffic detection are low cost and best for spot speed detection, while advanced radar sensors capable of multi-object tracking with higher accuracy and longer detection range are also available, they are very expensive and not widely used in traffic surveillance (McCoy, Bonneson, & Kollbaum, 1995). LiDAR sensors can provide 360-degree surveillance and generate precise 3D maps of the subject area, thus ideal for trajectory-level detection of all road users under complicated traffic conditions. High resolution LiDAR sensors such as 64- and 128-laser are still too expensive to deploy as mainstream means of infrastructure-based traffic detection, lower resolution products such as 16-laser currently cost about $4,000 per unit (Schubarth, 2018) and the price is still dropping. In the authors' opinion, lack of application is the main reason for the cost, other than the technic for production.

In terms of installation, traffic detection sensors are mainly divided into two categories: intrusive sensors which are mounted on or under the roadway surface (e.g., inductive loop) and nonintrusive sensors which are mounted to the side of the roadway on poles or other infrastructures (e.g., video cameras). Based on different detection objectives such as speed measurement, vehicle classification/counting, and queue detection, the size and shape of inductive loops are varied. The commonly used inductive loops include square loops (5ft or 6ft side length), round loops (6ft diameter), and rectangular loops (6ft width and variable length). The quality of deployment is important for inductive loops since unstable connections in pull boxes, wrong wire pairing, faulty sawcut cleaning and sealant application procedures can affect the reliability of sensing (Klein, Mills, Gibson, & Klein, 2006). For a video camera, its field of view is determined by focal length of lens, camera mounting height and viewing angle. Camera setup should avoid or minimize susceptibility to occlusion, reflected light and shadows that can lead to false or missed detection events. Usually, cameras used in traffic detection are mounted on luminaire masts (preferred because they are higher) or on the traffic signal masts (often on an extension arm) over the centers of the lanes being monitored (Klein, 2017).

LiDAR is a promising sensor in traffic detection whose features such as the number of channels, vertical field of view, and vertical resolution of lasers are all critical to its performance. Strategies for onboard installation have been studied by Premebida, Monteiro, Nunes, & Peixoto (2007), in which 0.65m above the ground was found to be the best position for pedestrians and automobile detection. While in Lizarazo Jimenez (2016), the LiDAR sensor was mounted atop a 1.2m extendable mast for the best performance. In the research of Kidono, Naito, & Miura (2012), the authors chose to mount a Velodyne 3D HDL-64ES2 LiDAR sensor on the roof of a passenger car, which was about 2.0m above the ground. Apparently, height and location are the two major considerations for onboard installations, and it depends on the purpose of the application. Manufacturers also provide guidance for onboard installation but in a very general way, for instance, Velodyne's manual simply depicts: 1) when the sensors are placed on the vehicle's roof in the fore and aft positions, the phase offsets are set to 180° and 0°; 2) when the sensors are mounted on the vehicle's roof in the left and right positions, the phase offsets are set to 90° and 270° (Velodyne, 2018).

Currently, guidance for roadside LiDAR installation could not be found in manufacturers' manual or literature. Zhao and Shibasaki (2005) were among the first in applying low-resolution LiDAR sensors at the roadside to detect pedestrians, according to their study, LiDAR sensors were placed about 0.2m above the ground, but the impact of installation on detection performance was not addressed. In another literature from the same authors, they placed six single-row SICK LMS2 LiDAR sensors on small chairs to perform scanning at a horizontal plane of about 0.4m above the ground (Zhao et al., 2012), again, the installation seemed to be arbitrary and the effectiveness was not addressed. Cooper, Raquet, & Patton (2018) examined the property of a Hokuyo UST-20LX LiDAR sensor for autonomous indoor navigation but also lacked insights on installation strategy. Therefore, in order to open a promising market segment for the LiDAR industry by introducing a new application field, it is necessary and urgent to explore how to select and install LiDAR sensors at the infrastructure side for better traffic detection performance.

In this paper, a detection range analysis of LiDAR sensors installed at the infrastructure side was discussed based upon both the sensor's built-in features and the installation techniques. The authors first conducted a theoretical study to analyze the best installation strategy such as location, height and inclination. Then three commonly used LiDAR sensor models were tested in the field under different height and inclination settings (with/without considering occlusion) to examine the theoretical results. At last, installation recommendations of single and multiple LiDAR sensors at a selected road segment were provided in a case study.

This paper is structured as follows: Section 2 introduces LiDAR sensors and LiDAR data. Section 3 presents the influential factors of LiDAR detection range in theoretical derivation. Section 4 discusses and evaluates the detection performance of three types of LiDAR sensors under different scenarios. Section 5 presents a case study in which installation recommendations of roadside LiDAR sensors are provided. Section 6 concludes the findings and future work.

## 2. LiDAR SENSOR AND DATA

A LiDAR instrument principally consists of a laser, a scanner, and a specialized GPS receiver. It creates 360-degree 3D point clouds representation of the surrounding environment in real time by rapidly spinning laser beams, which are mounted in a compact housing. Advanced digital signal processing and waveform analysis provide high accuracy, extended distance sensing, and calibrated reflectivity data.

There are two types of packets generated by the sensor: data packets and position packets (also called GPS packets). Data packets contain the 3D data measured by the sensor as well as the calibrated reflectivity of the surface from which the light pulse was returned. Also contained in the data packet is a set of azimuths, a four-byte timestamp, and two factory bytes identifying the model of the sensor and the return mode. The position packet provides an echo of the national Marine Electronics Association (NMEA) sentence received from an external time source as well as the pulse per second status and a time stamp representing the time when the position packet was assembled (Velodyne, 2016).

The rotation frequency (5 to 20Hz in general) of the LiDAR sensor can be customized by users. Obviously, the slower the LiDAR sensor rotates, the more data points can be collected. One data frame is generated after the sensor completes a 360-degree 3D scan and the collected point clouds are stored in the packet capture (pcap) format. The output data from a LiDAR sensor include the location of each point (in X, Y, Z coordinates) and their distance to the sensor, intensity, laser ID, azimuth, adjusted time, and timestamp. Based on the GPS location of the LiDAR sensor and a reference point, all the points can be matched to their exact locations in the real world. Fig. 1 shows a selected frame of raw 3D LiDAR point clouds collected by a 32-laser LiDAR sensor using a visualization software. Different colors of the data points represent the intensity/reflectivity of the objects. As shown, objects of interest such as vehicles, pedestrians, and road boundary, etc. can be clearly observed.

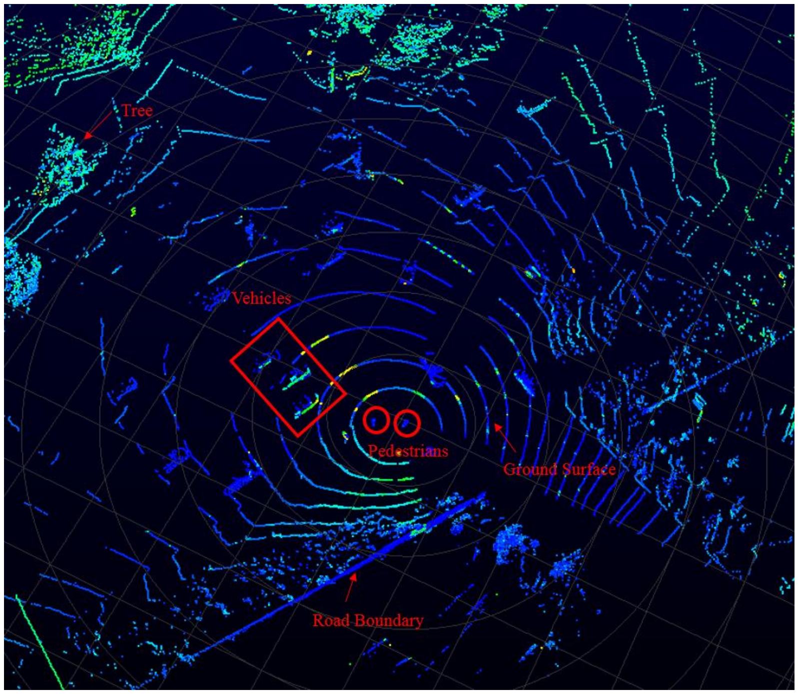


**Fig. 1.** Raw LiDAR point clouds collected by a 32-laser LiDAR.

## 3. INFLUENTIAL FACTORS OF LIDAR DETECTION PERFORMANCE

Based on the mechanical structure and operational principle of LiDAR sensors, laser beams are rotated 360-degree along the sensor's central axis to form a series of conical surfaces for scan. For a specific model, each laser channel is fixed at a specific elevation angle relative to the sensor's central axis. In Fig.2, two laser beams form their own conical surfaces independently. These lasers are divided into two groups: the lasers with a positive elevation angle ($\alpha_1$) and the lasers with a negative angle ($\alpha_2$). The perpendicular direction of the sensor's central axis is zero-degree. Since a laser beam travels along a straight line with a certain direction, the laser beams with positive angles can reach objects at a maximal distance as long as the reflected pulses can be collected, while the laser beams with negative angles cannot be used again after they shoot on the ground. They form a series of concentric circles on the ground and the LiDAR is projected at the center. In addition, the density of LiDAR point clouds is varied with the distance to the LiDAR sensor. If an object is located near the LiDAR, intensive data points are collected and thus presenting a fine description of the object. If an object is far away from the LiDAR, only sparse data points can be collected, especially for the small sized objects.

In traffic detection, the number of data points collected from road users is limited since majority of the data are unrelated background points. In this regard, the goals of traffic detection using roadside LiDAR sensors should be: 1) scan road users by as many laser beams as possible (i.e., collect as many data points as possible); 2) detect road users as far as possible. In the following sections, the authors will discuss in detail how a LiDAR model's built-in features and the installation strategy may affect its performance by using three popular types of LiDAR sensors as examples.

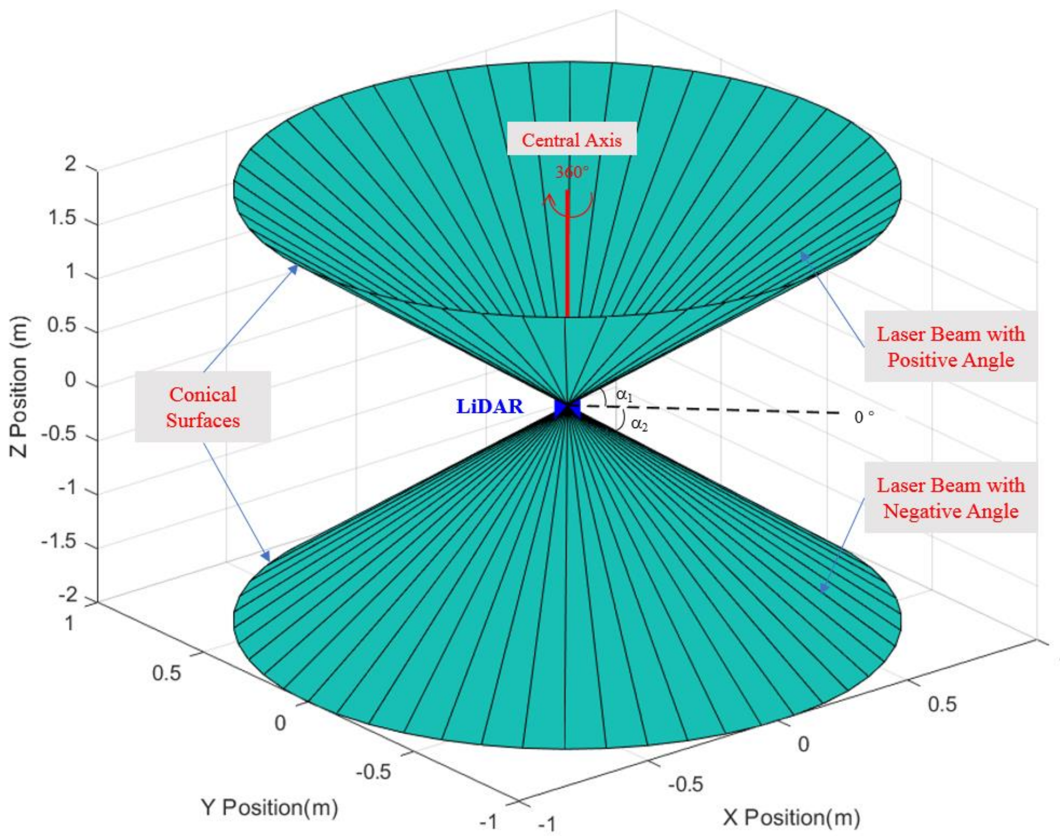


**Fig. 2.** Laser beams of LiDAR sensor.

### *3.1. LiDAR Built-in Features*

In order to choose proper LiDAR sensors, the primary features and specifications that need to be considered include channels, vertical field of view (FOV), and vertical resolution of laser beams. These three features can be configured and optimized according to the specific objective of LiDAR application. The definitions are summarized as follows:

(1) Channel: the total number of laser beams.

(2) Vertical FOV: sensor's vertical scan scope in degrees.

(3) Vertical Resolution: vertical angle between adjacent laser beams in degrees.

In general, the more laser channels, the more data points can be collected. The vertical FOV is determined by the number of channels and the vertical resolution of the laser beams. Table 1 lists the main features of three 360-degree LiDAR sensors from Velodyne company as examples. Puck and Puck Hi-Res LiDAR sensors have 16 laser beams and the vertical angle between adjacent laser beams is fixed. The Ultra Puck LiDAR sensor has 32 laser beams and the distribution of laser beams' vertical resolutions is non-linear.

**TABLE 1 Specifications of three selected LiDAR sensors.**

| **Name** | **Channels** | **Vertical FOV** | **Vertical Resolution** | **Measurement Range** | **Rotation Frequency** |
|---|---|---|---|---|---|
| Puck (VLP-16) | 16 | −15° to +15° (30°) | linear distribution (2°) | 100m | 5-20Hz |
| Puck Hi-Res | 16 | −10° to +10° (20°) | linear distribution (1.33°) | 100m | 5-20Hz |
| Ultra Puck (VLP-32C) | 32 | −25° to +15° (40°) | Non-linear distribution (0.33° for −4° to +1.33° FOV; Others are non-linear) | 200m | 5-20Hz |

### *3.2. LiDAR Installation*

Installation plays a pivotal role in determining the LiDAR's detection range and accuracy. Depends on the objective, LiDAR sensors can be temporarily installed on a tripod for short-term data collection or permanently mounted on roadside infrastructures for long-term data collection. While other factors also play their roles, the authors found the height and inclination are the two most influential factors.

#### *3.2.1. Installation Height*

The height of installation refers to the vertical distance between the LiDAR sensor and the ground surface. Without losing generality, we assume the gradient of the ground is zero-degree. How far the laser beams can reach is determined by the height of installation and the built-in features of the

LiDAR sensor, as well as the location and height of the target object. With respect to the occlusion issue, LiDAR sensors installed at a higher position can minimize the effect of occlusion; however, one should be aware it does not simply mean the higher the better because the undetectable area near the LiDAR sensor (such as the first undetectable pedestrian in Fig.3) may get larger if the LiDAR sensor is installed too high.

Fig. 3 illustrates a LiDAR sensor ($N$ = 8 channels, $\theta$ vertical field of view, and fixed $\delta$ vertical resolution of laser beams) horizontally installed at a height of $H$ above the ground. If the vertical angle of the lowest laser beam relative to the sensor's central axis is $\gamma_i$, then the farthest detection location of this laser beam is $H \times \tan \gamma_i$. The laser beams with positive angles can shoot as far as possible before reaching the object, while the detection range of the negative laser beams is $H \times (\tan \gamma_j - \tan \gamma_i)$, where the smallest and the largest vertical angle of negative laser beams are $\gamma_i$ and $\gamma_j$, respectively. A target object within the detection range cannot be guaranteed for detection since the height of the object should be larger than the height of the laser beams at the object's location, or the object will be missed (see the second undetectable pedestrian in Fig. 3).

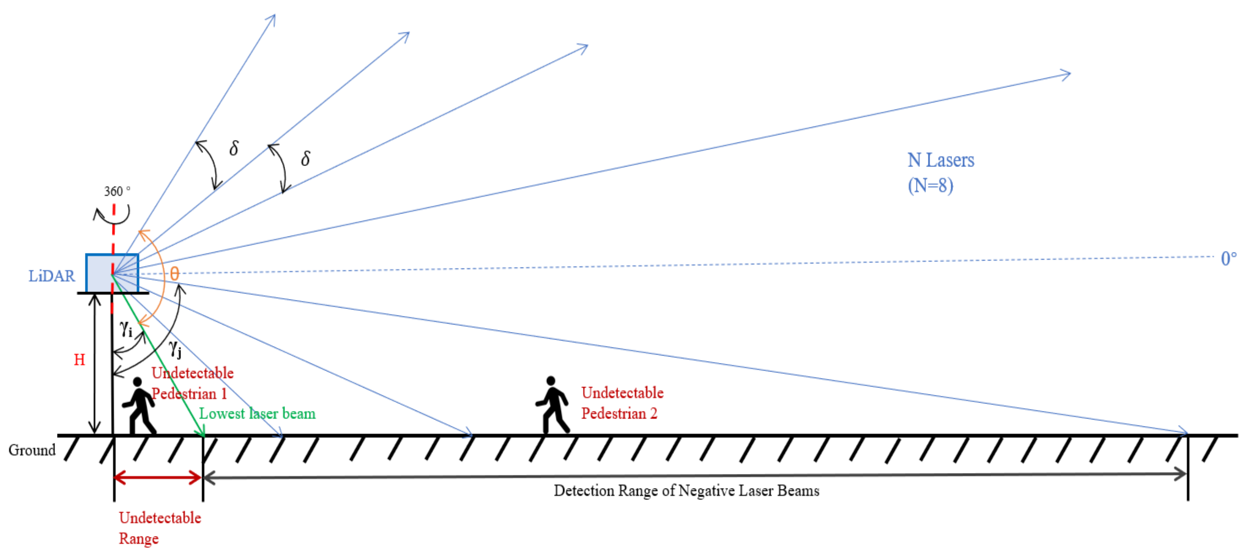


**Fig. 3.** Example of two undetectable scenarios.

### *3.2.2. Installation Inclination*

A LiDAR sensor can be mounted at any inclination angle, when it is placed on a horizontal plane, the sensor's central axis is perpendicular to the horizontal plane. Since all the laser beams are rotated along the sensor's central axis forming conical surfaces, target objects with the same distance to the sensor but in different orientations have been scanned identically because the angle of each laser beam relative to the horizontal plane is fixed. As shown in Fig. 4(a), the angle of the laser beam (AB or AC) relative to the horizontal plane is equal to $\alpha$ all the time during the 360° scan.

However, if we place a LiDAR sensor on a slope, the sensor's central axis is vertical to the surface of the slope. During the 360° scan, target objects with the same distance to the LiDAR sensor but in different orientations have been scanned differently. The reason for that is the angle of each laser beam relative to the horizontal plane is varied within the 360° scan. In Fig. 4(b), a LiDAR sensor is titled for $\beta$ degree relative to the vertical plane. Without an inclination, the angle between a laser beam (AB or AC) and the horizontal plane is $\alpha$ for 0° to 360° orientations. With an inclination, the projection of the laser beam on the horizonal plane is not a circle since AC>AB and EC>EB. It means that the detection range is decreased along the sensor's inclination direction. For example, the $\alpha$ changes to $\alpha+\beta$ and $\alpha-\beta$ at 0° and 180° orientations, respectively.

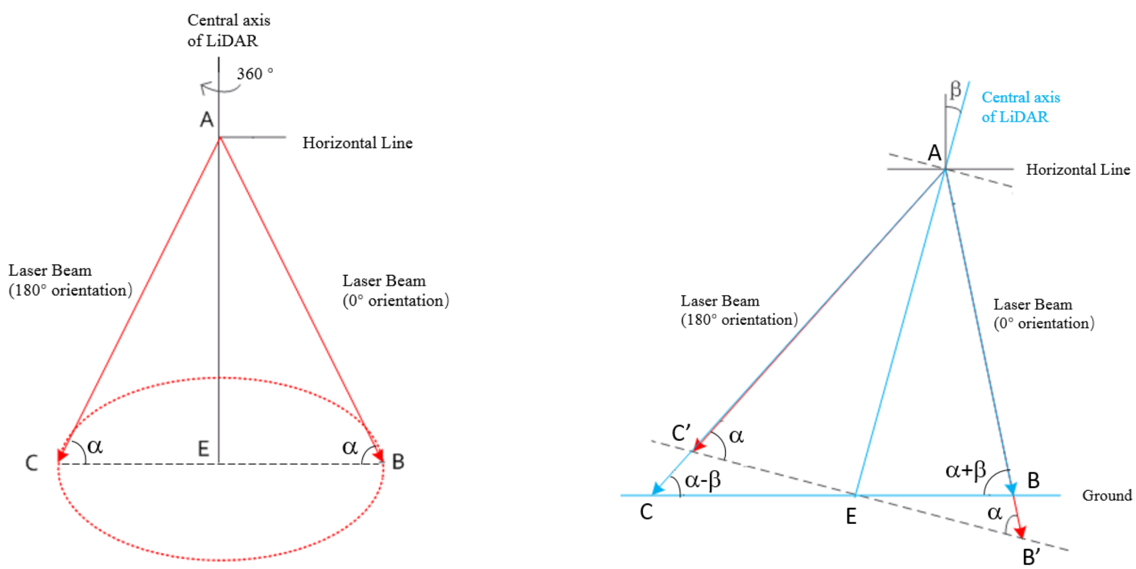


**(a).** Horizontal LiDAR **(b).** Inclined LiDAR

**Fig. 4.** Geometric demonstration of laser beams with/without LiDAR inclination.

*3.2.3. Theoretical Study*

The following is a theoretical derivation of the relationship between the laser beam's angle relative to the horizontal plane and the target object's orientation using an inclined LiDAR sensor. In Fig. 5, point A is the center of a LiDAR sensor. AX is the sensor's central axis, which has a relative inclination angle of $\beta$ to the vertical line AE (AE is perpendicular to the horizontal plane). A laser beam AB reaches AC after rotating $\theta$ degrees (assume the lengths of AB and AC are equal to $R$).

The angle $\gamma$ of the laser beam AB (or AC) relative to the AX is pre-defined by the LiDAR's specification.

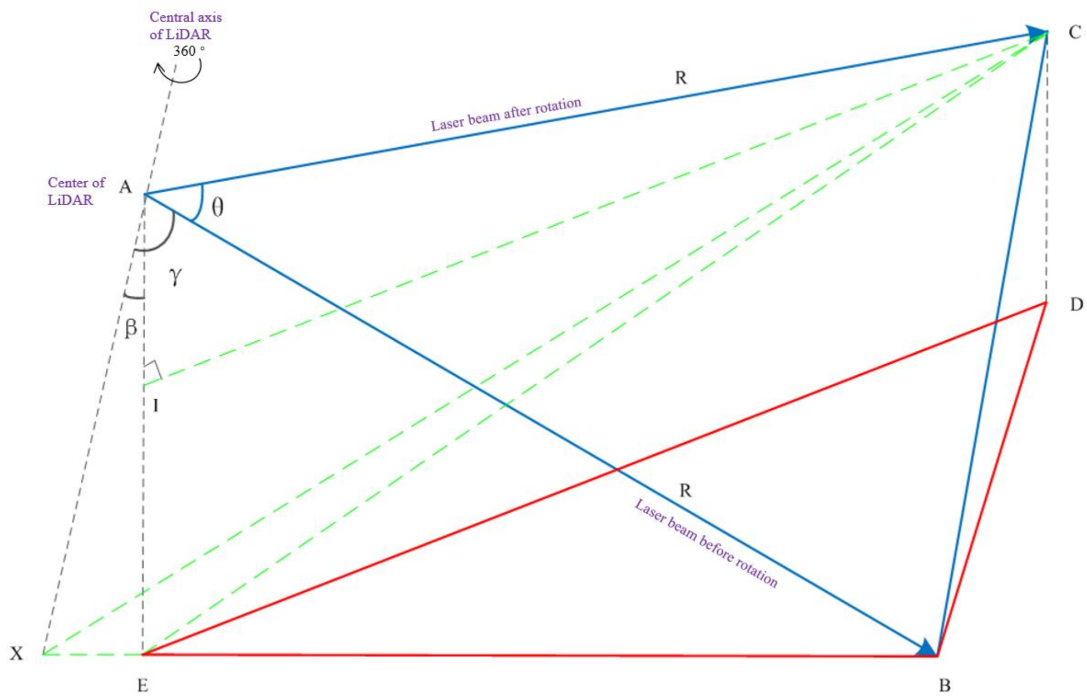


**Fig. 5.** Geometric demonstration of rotating laser beams with inclined LiDAR sensor.

**Given:** AB = AC = R (the length of laser beams)
$\angle$XAE = $\beta$ (LiDAR's inclination angle relative to the vertical line)
$\angle$XAB = $\angle$XAC = γ (the angle of laser beams relative to the sensor's central axis)
$\angle$BAC = $\theta$ (laser beam's rotation angle)

**Find:** 1) $\angle$ACI (the angle of the laser beam AC relative to the horizontal plane)
2) $\angle$DEB (the angle formed by projecting rotation angle $\theta$ to the horizontal plane)

In order to solve the above problem, we added several auxiliary lines: reversely extend BE to the sensor's central axis at point X; project point C to the horizontal plane as point D; CI is perpendicular to AE; connect XC, EB, ED, BC, and BD. Note that ΔEBD is the projection of ΔABC on the horizontal plane. Based on the spatial geometry, the angle of the laser beam AB relative to the horizontal plane can be defined, which is:

$$\alpha = \angle \mathrm{ABE} = 90° - \angle \mathrm{EAB} = 90° - (\angle \mathrm{XAB} - \angle \mathrm{XAE}) = 90° - \gamma + \beta \qquad \text{(Eq.1)}$$

**Calculate $\angle$ACI**

In Rt ΔAEB, $AE = Rsin\alpha, BE = Rcos\alpha$

In Rt ΔAEX, $XE = AEtan\beta$

In ΔXBC, $XC = XB = XE + BE$

In ΔABC, $BC = 2Rsin(\frac{\theta}{2})$

In ΔXBC, $\cos\left(\frac{\angle \mathrm{CXB}}{2}\right) = \frac{BC/2}{XC}$

In ΔXEC, $\cos(\angle \mathrm{CXB}) = \cos(\angle \mathrm{CXE}) = \frac{XC^2+XE^2-EC^2}{2XC \cdot XE}$

In ΔEAC, $\cos(\angle \mathrm{EAC}) = \frac{AE^2+AC^2-EC^2}{2AE \cdot AC}$

In Rt ΔAIC, $\angle \mathrm{ACI} = 90° - \angle \mathrm{EAC}$

Therefore, $\angle \mathrm{ACI} = 90° - \arccos\left(\cos(\gamma-\beta) - \tan\beta\left(2 - \frac{1-cos\theta}{\cos(\gamma-\beta)tan\beta+\sin(\gamma-\beta)}\right)\right)$ (Eq. 2)

**Calculate ∠DEB**

In Rt ΔAEX, $IE = AE - AI = AE - ACsin(\angle \mathrm{ACI})$

In rectangle ICDE, $CD = IE, DE = IC = ACcos(\angle \mathrm{ACI})$

In Rt ΔCDB, $DB^2 = BC^2 - CD^2$

In ΔDEB, $\cos(\angle \mathrm{DEB}) = \frac{DE^2+BE^2-DB^2}{2DE \cdot BE}$

Therefore, $\angle \mathrm{DEB} = \arccos\left(\frac{cos\theta - \cos(\gamma-\beta)\left(\cos(\gamma-\beta) - \tan\beta\left(2-\frac{1-cos\theta}{\cos(\gamma-\beta)tan\beta+\sin(\gamma-\beta)}\right)\right)}{\sin(\gamma-\beta)\sqrt{1-\left(\cos(\gamma-\beta)-\tan\beta\left(2-\frac{1-cos\theta}{\cos(\gamma-\beta)tan\beta+\sin(\gamma-\beta)}\right)\right)^2}}\right)$ (Eq. 3)

The next is a backward derivation of the previous problem. If the projection angle ∠DEB on the horizontal plane is given, how many degrees does the laser AB need to rotate?

**Given:** ∠DEB (the angle formed by projecting rotation angle $\theta$ to the horizontal plane)

∠XAE = $\beta$ (LiDAR's inclination angle)

∠XAB =∠XAC = $\gamma$ (the angle of laser beams relative to the sensor's central axis)

**Find:** 1) ∠BAC = $\theta$ (laser beam's rotation angle)

2) ∠ACI (the angle of the laser beam AC relative to the horizontal plane)

**Calculate θ and ∠ACI**

Define: $A = \sin(\gamma-\beta)$

$B = \cos(\gamma-\beta)$

$C = tan\beta$

$D = \cos(\angle \mathrm{DEB})$

$E = BC + A$

$x = cos\theta$

Then the Eq. 3 can be modified as $D = \frac{x - B(B - C\left(2 - \frac{1-X}{E}\right))}{A\sqrt{1-(B-C\left(2-\frac{1-X}{E}\right))^2}}$ (Eq. 4)

In Eq. 4, the values of the variable A, B, C, D, E are computable based on the given information. The only unknown variable is $x$. After mathematical simplification, Eq. 4 can be written as a quadratic equation of $x$ in a standard form:

$$\left(1 + \frac{B^2C^2 + A^2C^2D^2}{E^2}\right)x^2 +$$
$$\frac{2C}{E}\left(B - B^3 + 2B^2C - \frac{B^2C}{E} - A^2BCD^2 + 2A^2C^2D^2 - \frac{A^2C^2D^2}{E}\right)x +$$
$$B^2(B^2 - 2) + 2BC\left(2 - \frac{1}{E}\right)(1 - B^2) + B^2C^2(2 - \frac{1}{E})^2 - A^2D^2(1 - B^2 - 4C^2) +$$
$$2A^2BCD^2\left(2 + \frac{1}{E}\right) - \frac{A^2C^2D^2}{E}\left(4 - \frac{1}{E}\right) = 0 \quad \text{(Eq. 5)}$$

Using the Quadratic Formula, the value of $x$ can be obtained. Since $x$ is equal to $cos\theta$, $\theta$ is known. In addition, if we substitute $x$ for the $cos\theta$ in Eq. 2, ∠ACI can also be calculated.

Fig. 6 shows an example to demonstrate the application of the above derivation. When a LiDAR sensor is installed horizontally ($\beta = 0°$), the angle of a laser beam relative to the horizontal plane is 3° ($\alpha = 3°$), that is, $\gamma = 90° - \alpha + \beta = 87°$. No matter which orientation a target object is located (∠DEB $= 0°\sim360°$), the angle of the same laser beam relative to the horizontal plane is fixed: ∠ACI $= \alpha = 3°$. However, if we title the LiDAR sensor $\beta = -1°$, then the ∠ACI is changed with different orientations. For example, when a target object is located at 0° (∠DEB $=$ 0°) orientation relative to the LiDAR sensor, the angle of the same laser beam relative to the horizontal plane is changed from 3° to 2° (∠ACI $= 2°$); When the same target object is located at 180° (∠DEB $= 180°$) orientation, the angle is changed from 3° to 4° (∠ACI $= 4°$). Two intermittent points at 90° and 270° orientations are due to the undefined Tangent function used in the calculation equations.

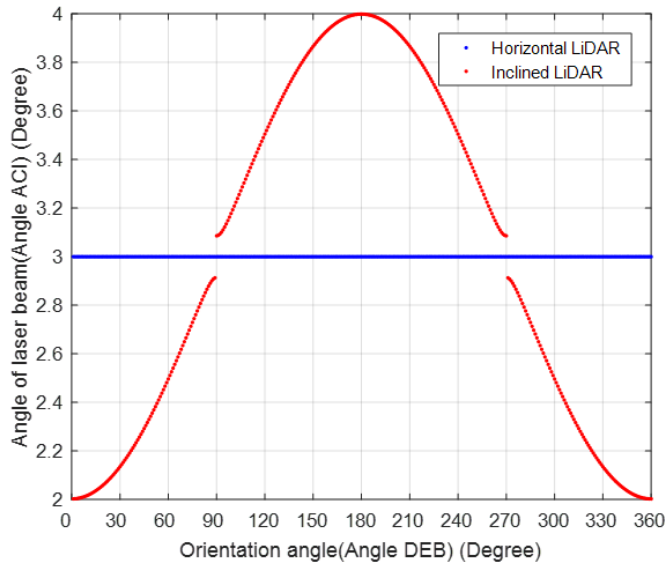


**Fig. 6.** Angle variation with horizontal and inclined LiDAR sensor.

### *3.3. Occlusion*

Occlusion is always a problem in reality. A vehicle or a pedestrian can be fully or partially blocked by other road users. Large objects may also locate near the LiDAR sensor. Under these circumstances, the number and distribution of laser beams shooting at the target object may be changed since the laser beams cannot penetrate the front obstructions and continue to shoot at the target object. The level of occlusion is affected by the LiDAR's built-in features and installation, the relative location and height of the target object and obstructions. Assuming that the number of valid laser beams shooting at the target object without and with occlusion is $n_r$ and $n_o$, respectively, then the detection loss percentage of the target object due to occlusion is calculated by Eq. 6.

$$Loss\ Percentage = \left(1 - \frac{n_o}{n_r}\right) \times 100\% \qquad \text{(Eq. 6)}$$

Fig. 7 demonstrates the occlusion issue using a Puck LiDAR sensor as an example: a 1.5m height obstruction is fixed at a 5.0m location, while a 1.0m height target object is moving within the detection range of the sensor. Note that in the plot, the ranges of X and Y axes have a big difference, so it seems that the angles between adjacent lasers are not the same. In fact, the resolution of the laser beams is fixed (2° for Puck sensor). At the location A, the target object is fully blocked by the obstruction (loss percentage = 100%); At the location B, the target object is partially blocked by the obstruction (loss percentage = 50%); At the location C, even though the target object is located behind the obstruction, the detection of the target object is not affected by the obstruction since the valid laser beams are different (loss percentage = 0%).

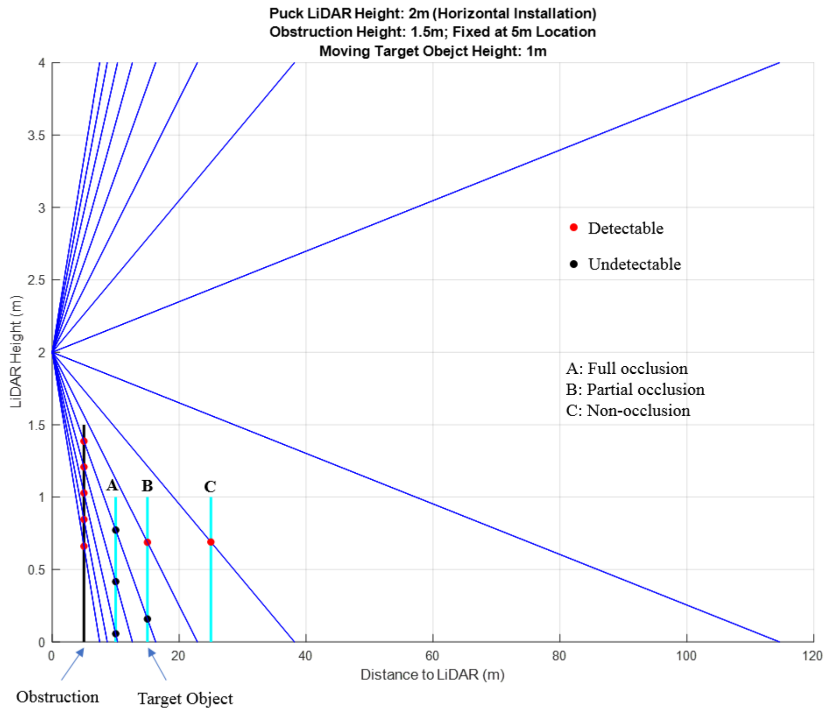


**Fig. 7.** Demonstration of object detection with consideration of occlusion.

### *3.4. Assessment of LiDAR Detection Performance*

Even though LiDAR manufacturers provide specifications on the measurement range of each model, it does not mean an object located at the farthest measurement distance can be correctly identified for sure, especially for the small sized objects. For example, the detection range of Puck LiDAR sensors is up to 100 meters according to the user manual (Velodyne, 2016). However, based on our previous studies (Zhao et al., 2019), stably valid detection/identification range of vehicles and pedestrians of this model was only about 30 to 35 meters in one direction (i.e., a circle with 30-35m radius). In order to identify the object types (e.g., pedestrians or vehicles) correctly, at least two or three laser beams need to shoot at the target object. In this paper, two criteria used for assessing LiDAR detection performance are: 1) how many valid laser beams can shoot at the target object; 2) the vertical height between two adjacent valid laser beams shooting at the target object.

Given that a $N$-laser LiDAR sensor is installed at a height of *hLiDAR* meters above the flat ground and the inclination angle is $\beta$ degree. The vertical angle of each laser beam relative to the sensor's central axis is $\gamma_i$ $(i = 1, 2, \ldots, N)$ degree. A target object (height: *hObject* meters) is located at $\varphi$ degree orientation with *dObject* meters away from the LiDAR. An obstruction (height: *hBlockObject* meters) is located at $\varphi_b$ degree orientation with *dBlockObject* meters away from the LiDAR. The total number of laser beams ($n$) shooting at the target object and the vertical height ($\Delta Y$) between two adjacent valid laser beams can be calculated by Algorithm 1.

---

**Algorithm 1: LiDAR detection performance assessment.**

**Input**: hObject, dObject, hBlockObject, dBlockObject, hLiDAR, N, $\varphi$, $\varphi_b$, β, γ

**Output**: n, ΔY

---

Begin

If obstruction exists // For occlusion case

  For j = 1:N

    $\theta_b \leftarrow$ Eq. 5 $(\varphi_b, \beta, \gamma_j)$ // The laser beam's rotation angle ($\cos\varphi_b = \mathrm{D}, \cos\theta_b = x$ in Eq. 5)

    $\gamma_{jb}{}' \leftarrow$ Eq. 2 $(\theta_b, \beta, \gamma_j)$ // The vertical angle of laser beam relative to the horizontal plane ($\gamma'_{jb} = \angle$ACI in Eq. 2)

    $x_{jb} \leftarrow$ dBlockObject // Equation for obstruction

    $y_{jb} \leftarrow \tan(\gamma'_{jb}) \cdot x_{jb} + hLiDAR$ // Equation for laser beam

    If $0 \leq y_b \leq$ hBlcokObject // Shooting at the obstruction

      $\gamma_b \leftarrow \gamma_j$ // Save vertical angles of the used laser beams

    Endif

  Endfor

  $\gamma_{valid} \leftarrow \gamma - \gamma_b$ // The vertical angles of remaining laser beams

Else

  $\gamma_{valid} \leftarrow \gamma$ // For non-occlusion case

Endif

count $\leftarrow$ 0

For i = 1:N

$\theta \leftarrow$ Eq. 5 $(\varphi, \beta, \gamma_{valid,i})$

$\gamma_i{}' \leftarrow$ Eq. 2 $(\theta, \beta, \gamma_{valid,i})$

$x_i \leftarrow$ dObject // Equation for target object

$y_i \leftarrow \tan(\gamma_i') \cdot x_i + hLiDAR$

If $0 \leq y_i \leq$ hObject

count $\leftarrow$ count + 1

Endif

Endfor

$\Delta Y = | y_i - y_{i-1} |$ // Vertical height between two adjacent valid laser beams

n $\leftarrow$ count

Return: n, $\Delta Y$

---

For multiple LiDAR sensors, each sensor works independently. If a target object is located within the overlapped detection areas of multiple sensors, the valid number of laser beams shooting at the target object can be accumulated. Details of multiple sensor integration will be demonstrated in Case Study.

## 4. DETECTION RANGE ANALYSIS

After theoretical analysis has been presented, attention now can be directed to experimental studies, in which three types of commonly used LiDAR sensors (Puck, Puck Hi-Res, and Ultra Puck) were applied at installation sites (as shown in Fig. 8) to examine the theoretical results. The sensors were mounted on a tripod for easy adjustment of the height and inclination angle. A scale rod, a protractor, and a distance ruler were used to measure the height and inclination as well as the horizontal distance to the LiDAR sensor. Whiteboards with different dimensions were used to represent objects with different sizes.


**Fig. 8.** Data collection in a parking lot.

### *4.1. Different Heights & Horizontal Installation*

Case description: a LiDAR sensor was horizontally installed at a height of 1.5m, 1.8m, and 2.0m above the flat ground, the height of a moving target object was 1.8m. Since the LiDAR senor did not have an inclination angle, the orientation of the objects which had a same distance to the LiDAR sensor was not an influential factor of LiDAR detection range in this scenario. Table 2 lists the detection range of the three selected LiDAR sensors with different heights. For the same type of the LiDAR sensor, it is clearly shown that different heights of the sensor would lead to different detection ranges.

**TABLE 2 Detection Range of LiDAR Sensors (Horizontal Installation).**

| LiDAR | Height (m) | Detection Range (m) | | |
|---|---|---|---|---|
| | | ≥ 1 laser | ≥ 2 lasers | ≥ 3 lasers |
| Puck | 1.5 | 1.0-85.5 | 1.0-28.5 | 1.0-17.0 |
| | 1.8 | 1.0-100.0 | 1.0-34.0 | 1.0-20.5 |
| | **2.0** | **1.0-100.0** | **1.0-38.0** | **1.5-22.5** |
| | | | | |
| Puck Hi-Res | 1.5 | 1.0-100.0 | 1.0-43.0 | 1.0-25.5 |
| | 1.8 | 1.0-100.0 | 1.0-51.5 | 1.0-30.5 |
| | 2.0 | 1.5-100.0 | 1.5-57.0 | 2.0-34.0 |
| | | | | |

| | | | | |
|---|---|---|---|---|
| Ultra Puck | 1.5 | 1.0-200.0 | 1.0-200.0 | 1.0-128.5 |
| | 1.8 | 1.0-200.0 | 1.0-200.0 | 1.0-154.5 |
| | 2.0 | 1.0-200.0 | 1.0-171.5 | 1.0-114.5 |

Note: The height of a target object is 1.8m.

The heatmaps in Fig. 9 show the detection performance of a Puck sensor which was horizontally installed at a height of 2.0m as an example. In the left plot, the color of each cell in the heatmap represents the valid number of laser beams ($n$) shooting at the target object. In the right plot, the color of each cell in the heatmap indicates the vertical height ($\Delta Y$) between two adjacent valid laser beams shooting at the target object. With the distance between the target object and the sensor increases, the value of $n$ decreases and the $\Delta Y$ increases because the scan planes of the LiDAR sensor are a series of conical surfaces.

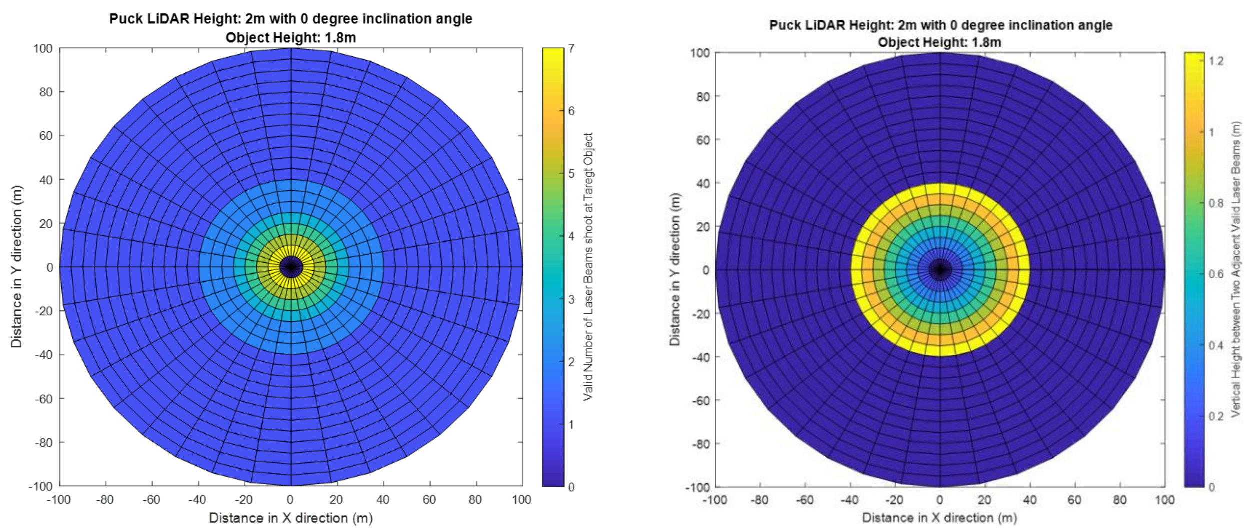


**Fig. 9.** Heatmaps of Puck LiDAR sensor (horizontal installation).

### *4.2. Fixed Height & Inclined Installation*

Case description: a LiDAR sensor was installed at a fixed 2.0m height above the flat ground and the sensor's inclination angle was $-1°$ to $+2°$ with $1°$ resolution, the height of a moving target object was 1.8m. Since the LiDAR sensor was tilted, the objects located at different distances and orientations relative to the LiDAR sensor were scanned diversely. The heatmaps in Fig. 10 show the detection pattern changes of a Puck LiDAR sensor when the inclination angle was varied from $-1°$ to $+2°$. Fig.11 demonstrates the detection performance of Puck Hi-Res and Ultra Puck sensors with $\pm 1°$ inclination. For an individual heatmap, the plot is symmetric about the X-axis;

For a pair of heatmaps from the same LiDAR sensor with the same inclination angle but in opposite directions (e.g., ±1°), two corresponding heatmaps are centrosymmetric.

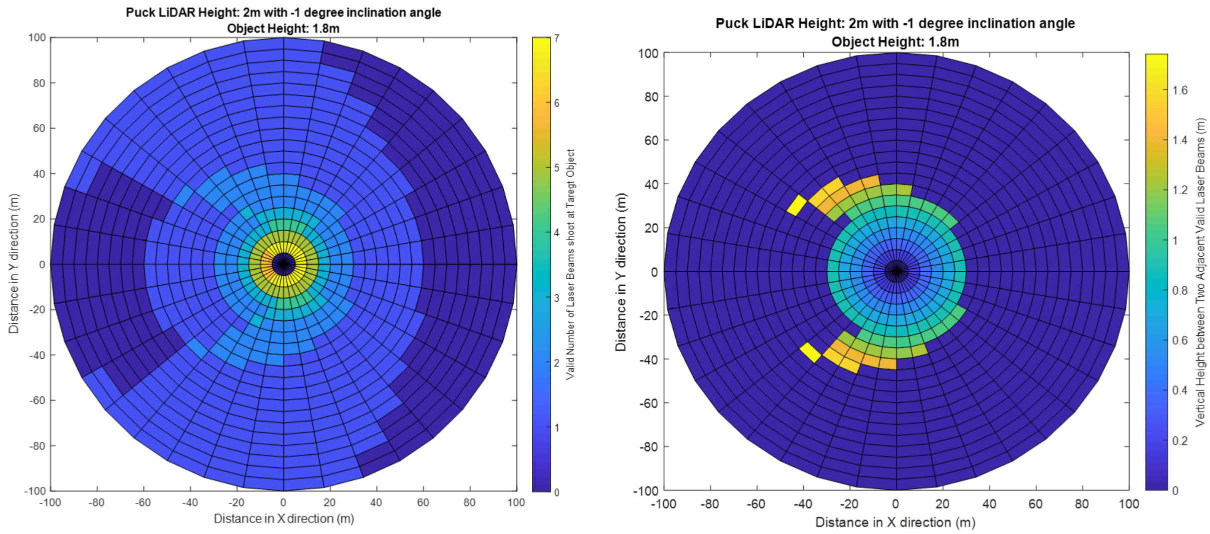


**(a).** Heatmaps of Puck LiDAR sensor with -1° inclination.

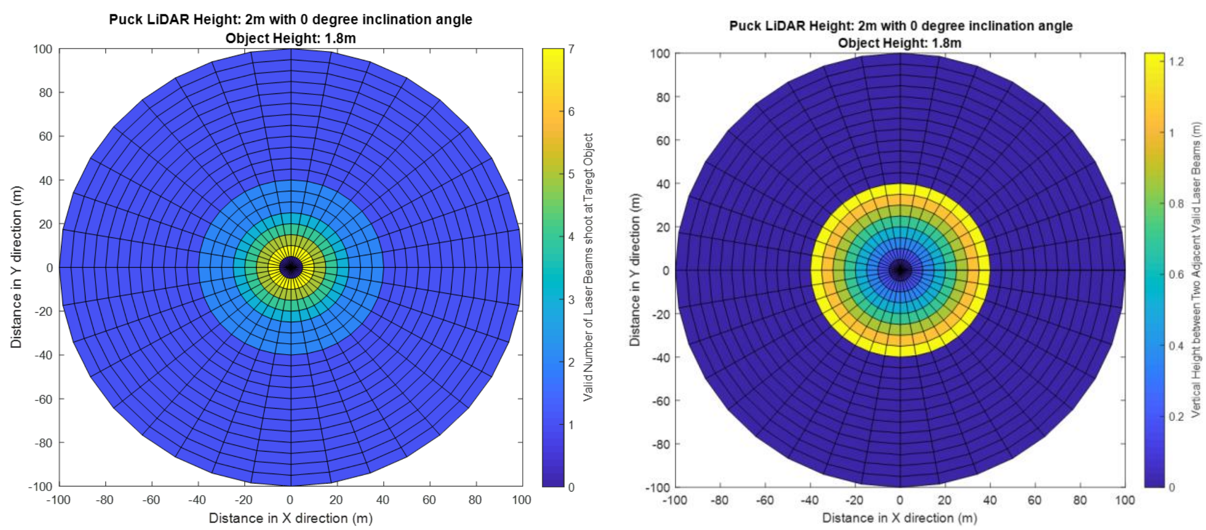


**(b).** Heatmaps of Puck LiDAR sensor with 0° inclination.

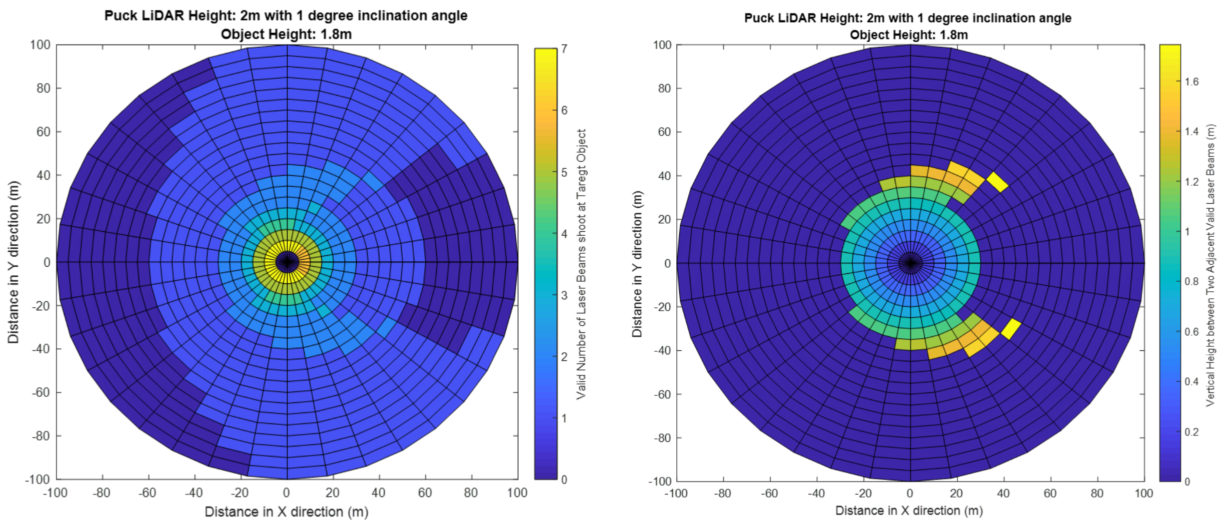


**(c).** Heatmaps of Puck LiDAR sensor with +1° inclination.

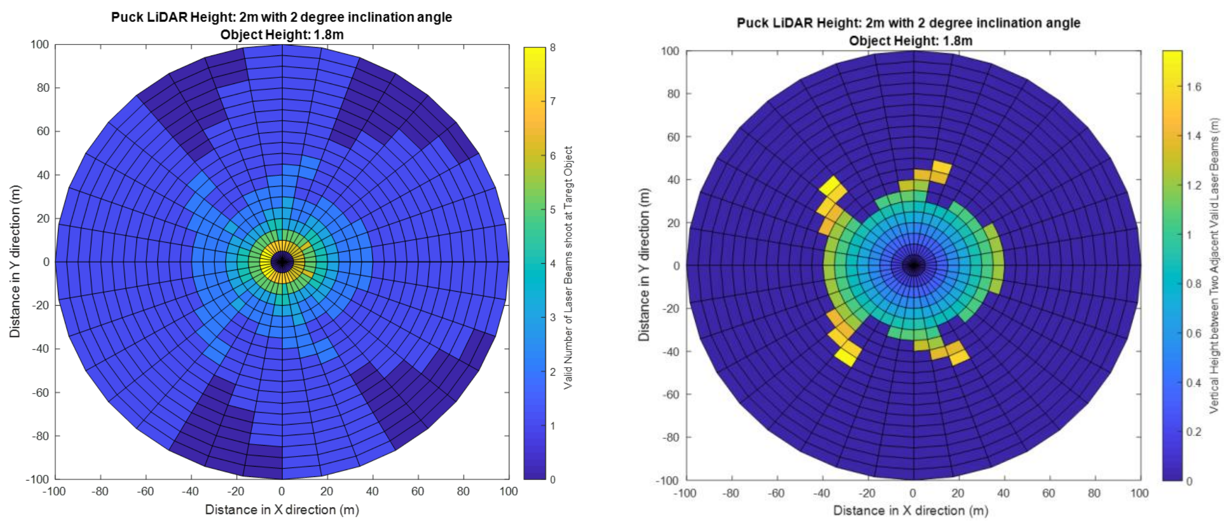


**(d).** Heatmaps of Puck LiDAR sensor with +2° inclination.

**Fig. 10.** Heatmaps of Puck LiDAR sensor (inclined installation).

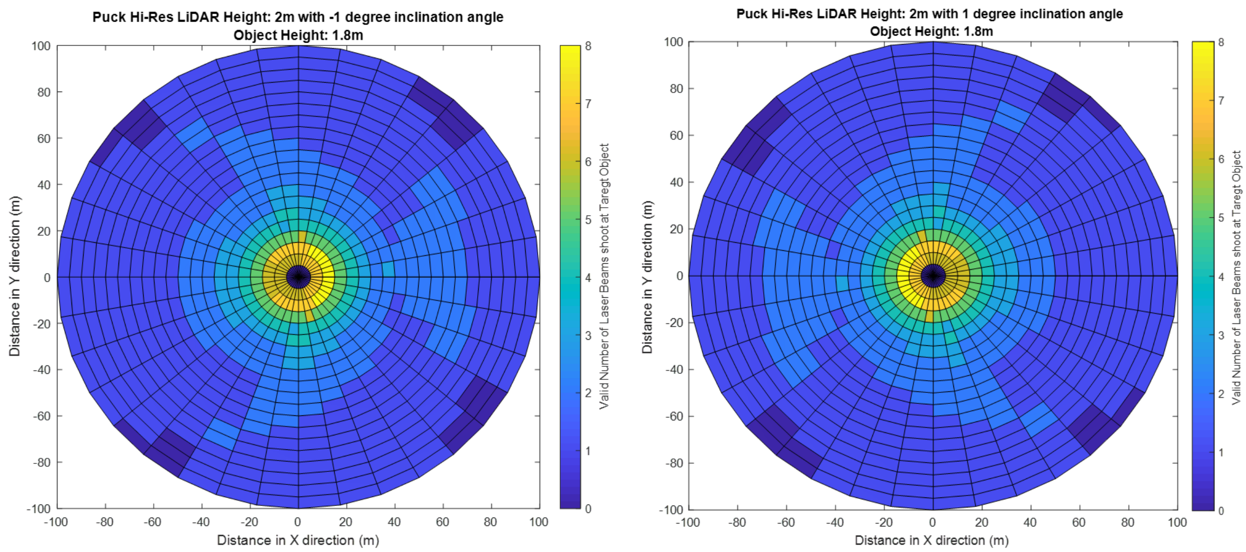


**(a).** Heatmaps of Puck Hi-Res LiDAR sensor with ±1° inclination.

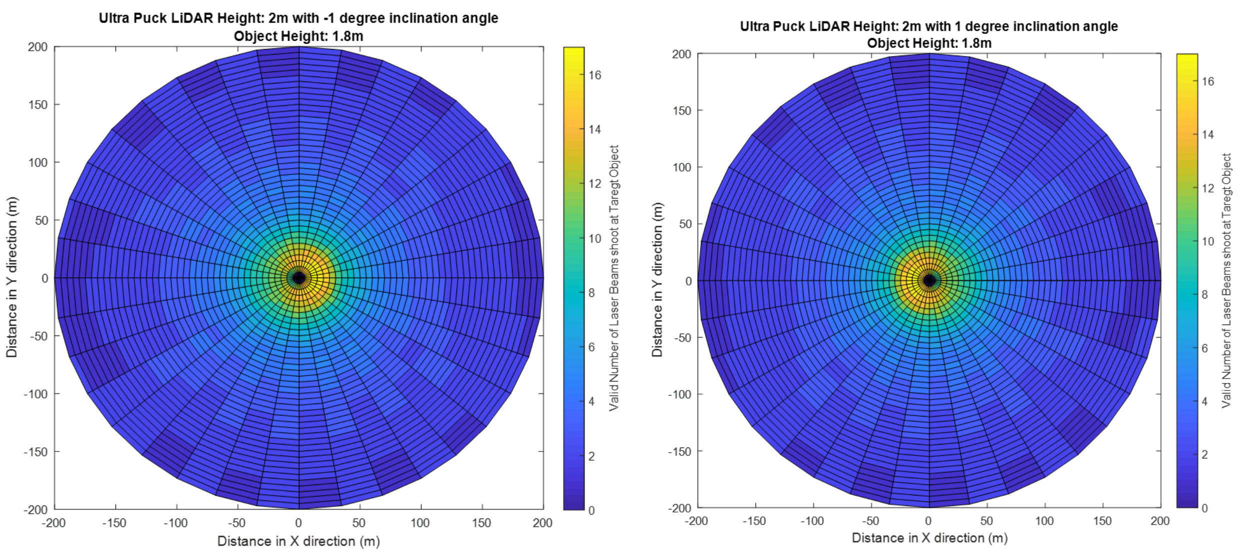


**(b).** Heatmaps of Ultra Puck LiDAR sensor with ±1° inclination.

**Fig. 11.** Heatmaps of Puck Hi-Res and Ultra Puck LiDAR sensors (inclined installation).

### *4.3. Special Case: Fixed Height & Vertical Installation*

Case description: a LiDAR sensor was installed at a fixed height above the flat ground and the sensor's inclination angle was 90° (i.e., vertical installation). In this case, the sensor's central axis was parallel to the horizontal plane, thus during the 360° scan, the downward 180° scan and the upward 180° scan were valid for detecting objects on the ground and in the air, respectively.

The authors conducted a field experiment in a warehouse to test this special case: a Puck LiDAR sensor with a 90° vertical inclination angle was installed on a horizontal pole to scan the warehouse's ceiling (as shown in Fig. 12). The height from the ceiling to the LiDAR sensor was about 5.13m and the direction of the ceiling surface was perpendicular to the sensor's central axis. Under this vertical deployment condition, 16 laser beams shot at different locations of the ceiling surface during one 360° scan (as shown in Fig. 13). Based on the theoretical derivation in the previous sections, the scan locations of the ceiling surface by a vertically installed Puck LiDAR senor at a fixed height are determined (as shown in Fig. 14). To validate the calculation, the authors randomly chose 16 locations along the X-axis (one specific location from each laser beam) and compared the widths along the Y-axis obtained from the calculation and the measurement. Table 3 lists the validation results and corresponding offsets. It showed that the average measurement accuracy of the field data was about 3.5cm and the relative offset was 1.6%. According to the user manual of Puck sensors (Velodyne, 2016), the measurement accuracy of this type of LiDAR sensor is about 3.0cm, which verified the result of the theoretical study. The measurement accuracy of the ceiling's height and the vertical deployment of the LiDAR sensor are the potential reasons for the offsets. Besides, we found that the laser beams with smaller vertical angles have better accuracy than those with larger vertical angles, and this issue may be caused by: 1) the LiDAR manufacturer does not provide information for angular correction; 2) at a same horizonal location/distance from the LiDAR sensor, laser beams with larger vertical angles travel longer distance before shooting at the ceiling than that propagated by laser beams with smaller angles, thus there is a higher probability of giving measurements with lower accuracy.

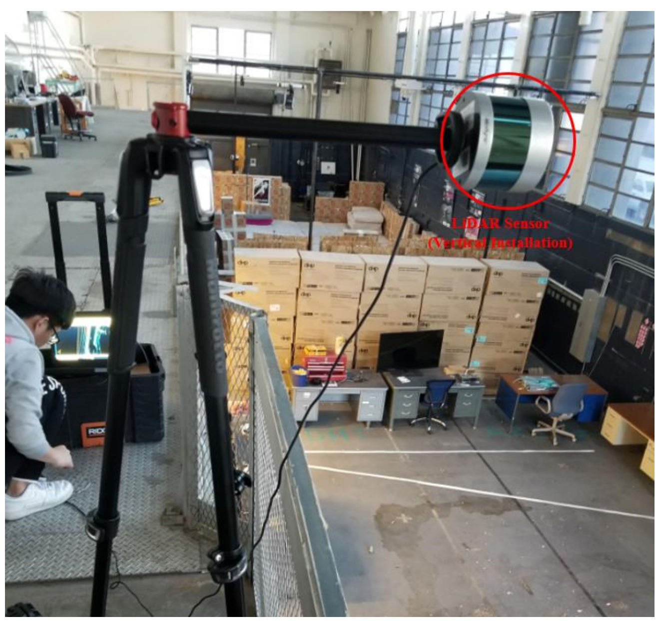


**Fig. 12.** Data collection in a warehouse.

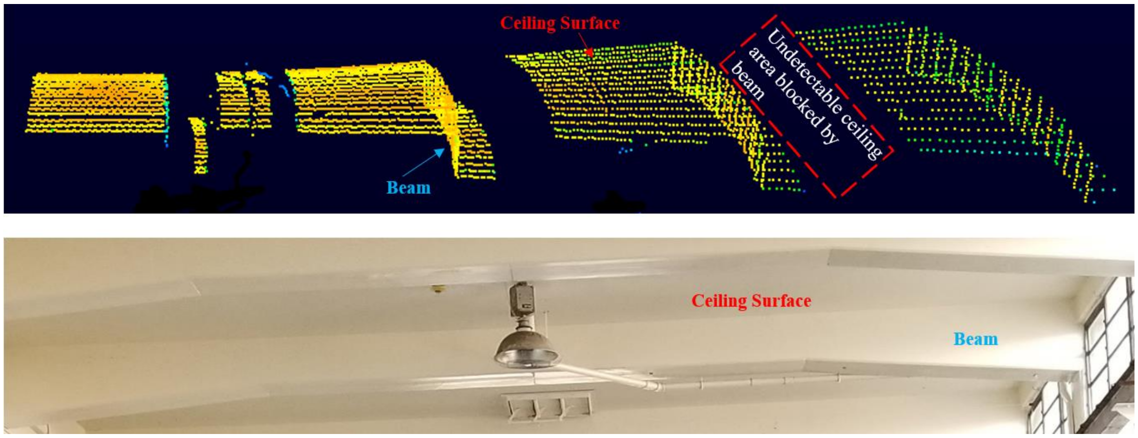


**Fig. 13.** Scanned ceiling surface viewed in a visualization software and in reality.

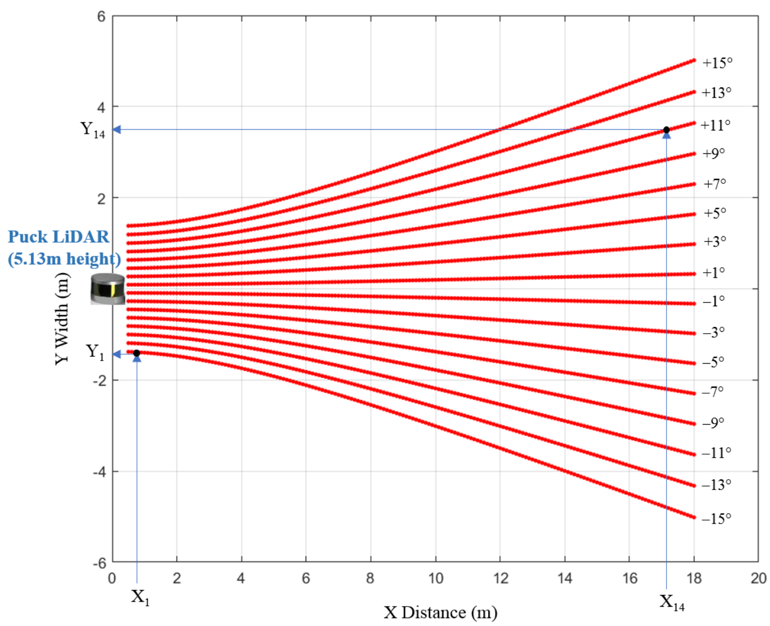


**Fig. 14.** Calculated scan locations of the ceiling surface by a Puck LiDAR sensor (vertical installation).

## TABLE 3 Validation for Scan Location Calculation

| Laser Angle (degree) | Distance (m) | Calculated Width (m) | Measured Width (m) | Absolute Offset (m) | Relative Offset (%) |
|---|---|---|---|---|---|
| −15 | 0.767 | −1.390 | −1.357 | 0.033 | 2.374 |
| −13 | 2.663 | −1.335 | −1.303 | 0.032 | 2.397 |
| −11 | 3.137 | −1.169 | −1.147 | 0.022 | 1.882 |
| −9 | 3.622 | −0.995 | −0.982 | 0.013 | 1.307 |
| −7 | 4.468 | −0.835 | −0.828 | 0.007 | 0.838 |
| −5 | 5.658 | −0.668 | −0.666 | 0.002 | 0.299 |
| −3 | 6.370 | −0.429 | −0.428 | 0.001 | 0.233 |

| | | | | | |
|---|---|---|---|---|---|
| –1 | 7.158 | –0.154 | –0.154 | 0.000 | 0.000 |
| +1 | 9.595 | 0.190 | 0.192 | 0.002 | 1.053 |
| +3 | 10.363 | 0.606 | 0.615 | 0.009 | 1.485 |
| +5 | 11.365 | 1.091 | 1.109 | 0.018 | 1.650 |
| +7 | 13.517 | 1.775 | 1.812 | 0.037 | 2.085 |
| +9 | 14.661 | 2.460 | 2.516 | 0.056 | 2.276 |
| +11 | 17.270 | 3.502 | 3.592 | 0.090 | 2.570 |
| +13 | 17.656 | 4.245 | 4.356 | 0.111 | 2.615 |
| +15 | 17.957 | 5.004 | 5.137 | 0.133 | 2.658 |
| | | | **Average** | **0.035** | **1.608** |

### *4.4. Occlusion Case*

Case description: a LiDAR sensor was installed at a height of 1.5m, 2.0m, and 2.5m above the flat ground. The heights of obstructions were set to 0.5m, 1.0m, 1.2m, and 1.5m. Two target objects with 1.0m and 1.5m height were used as moving objects to test the level of occlusion due to the obstruction. In each case, the obstruction was set at a fixed location (5.0m, 10.0m, 15.0m, 20.0m, and 25.0m) from the LiDAR sensor.

Based on our previous research experience, correct object identification needs at least two laser beams shooting at the object. Table 4 summarizes the valid detection range (≥ 2 laser beams) of the selected Puck sensor in three representative cases. For example, a Puck LiDAR sensor was horizontally installed at a 2.0m location. A 1.0m height obstruction was located 10.0m from the sensor and a 1.5m height target object was moving within a range of 100.0m from the sensor. In Fig. 15, the red line represents the valid number of laser beams at each location of the target object. The blue bar shows the detection loss percentage of the target object. The two gray areas (3-22m, 29-38m) indicate the valid detection ranges where at least two laser beams can shoot at the given target object.

**TABLE 4 Detection Range of Puck LiDAR Sensor Considering Occlusion**

| **$h_{object}$ = 1.5m, $h_{LiDAR}$ = 2.0m (horizontal)** | | | | |
|---|---|---|---|---|
| **$h_{BlockObject}$** / **$d_{BlockObject}$** | Detection Range (≥ 2 lasers) (m) | | | |
| | 0.5m | 1.0m | 1.2m | 1.5m |
| 5.0m | 3-22, 29-38 | 3-22, 29-38 | 3-22, 29-38 | 3-4, 10-22, 29-38 |
| 10.0m | 3-22, 29-38 | **3-22, 29-38** | 3-9, 29-38 | 3-9 |
| 15.0m | 3-22, 29-38 | 3-14, 29-38 | 3-14, 29-38 | 3-14 |
| 20.0m | 3-19, 29-38 | 3-19 | 3-19 | 3-19 |
| 25.0m | 3-22, 29-38 | 3-22 | 3-22 | 3-22 |

| $h_{object}$ = 1.0m, $h_{LiDAR}$ = 2.0m (horizontal) | | | | |
|---|---|---|---|---|
| $h_{BlockObject}$ / $d_{BlockObject}$ | Detection Range (≥ 2 lasers) (m) | | | |
| | 0.5m | 1.0m | 1.2m | 1.5m |
| 5.0m | 5-16, 20-22 | 7-17, 20-22 | 9-16, 20-22 | 20-22 |
| 10.0m | 5-9, 12-16, 20-22 | 5-9, 20-22 | 5-9 | 5-9 |
| 15.0m | 5-14, 20-22 | 5-14 | 5-14 | 5-14 |
| 20.0m | 5-16 | 5-16 | 5-16 | 5-16 |
| 25.0m | 5-16, 20-22 | 5-16, 20-22 | 5-16, 20-22 | 5-16, 20-22 |
| $h_{object}$ = 1.5m, $h_{LiDAR}$ = 2.5m (horizontal) | | | | |
| $h_{BlockObject}$ / $d_{BlockObject}$ | Detection Range (≥ 2 lasers) (m) | | | |
| | 0.5m | 1.0m | 1.2m | 1.5m |
| 5.0m | 5-28 | 5-28 | 6-28 | 7-28 |
| 10.0m | 5-28 | 5-9, 12-28 | 5-9,12-28 | 5-9, 20-28 |
| 15.0m | 5-28 | 5-14, 20-28 | 5-14 | 5-14 |
| 20.0m | 5-28 | 5-19 | 5-19 | 5-19 |
| 25.0m | 5-24 | 5-24 | 5-24 | 5-24 |

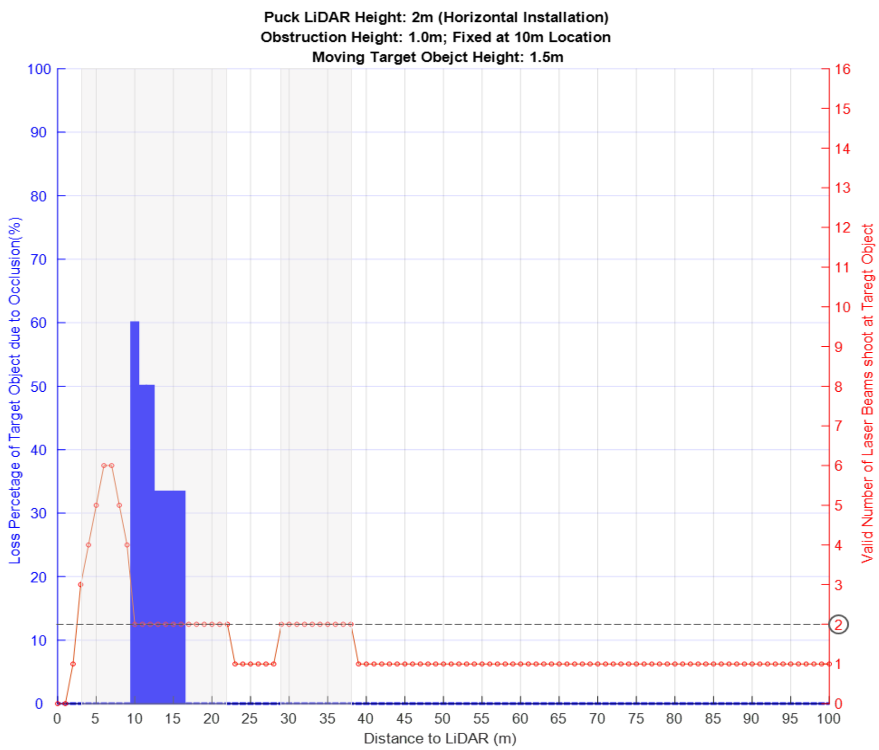


**Fig. 15.** Demonstration of Puck sensor's detection performance considering occlusion.

## 5. CASE STUDY

In this section, the authors provide installation recommendations of three commonly used LiDAR sensors for detecting and tracking vehicles along a six-lane highway. The geometric design of the selected road segment is shown in Fig. 16 and the LiDAR sensor was designed to install at the median (39.554N, –119.788W).

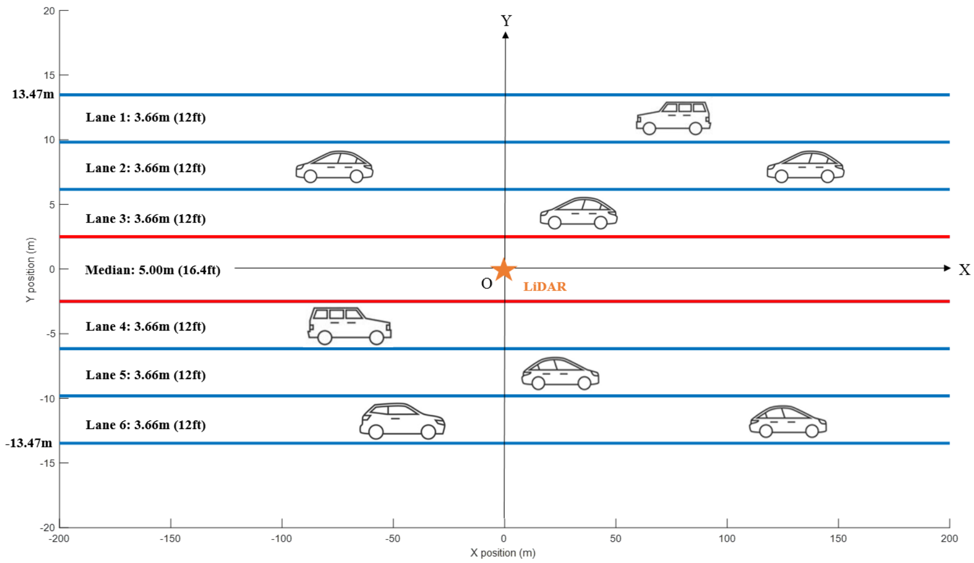


**Fig. 16.** Geometric design of the selected road segment.

In order to obtain good detection performance of vehicles along a target road segment with certain lane and width, how to find appropriate installation height and inclination of the LiDAR sensor is an optimization problem. Based on the Section 3 and 4, we defined the objective function was to maximize the sensor's total detection areas where at least two laser beams can shoot at the vehicles with average height.

Define: The LiDAR senor's height is $h_{LiDAR}$ (m) within a range of [$H_{min}$, $H_{max}$] (m).

The LiDAR senor's inclination is $\beta$ (degree) within a range of [$A_{min}$, $A_{max}$] (degree).

The size of the study area is [$X_{min}$, $X_{max}$, $Y_{min}$, $Y_{max}$] (m).

The total number of cells in heatmap is $T$.

The area of each cell in heatmap is $S_i$ (i = 1, 2, …,T) ($m^2$)

The valid number of laser beams in each cell is $n_i$ (i = 1, 2, …,T).

The Cartesian location of each cell in heatmap is ($x_i$, $y_i$), (i = 1, 2, …,T) (m).

The required minimal number of valid laser beams in each cell is *MinLaserCount*.

Objective Function: max $\sum_{i=1}^{T} S_i$

Subject to: 1) $n_i \geq MinLaserCount$

2) $X_{min} \leq x_i \leq X_{max}$

3) $Y_{min} \leq y_i \leq Y_{max}$

4) $H_{min} \leq h_{LiDAR} \leq H_{max}$

5) $A_{min} \leq \beta \leq A_{max}$

6) $i = 1, 2, \ldots, T$

According to the actual situation in the field, the single LiDAR sensor was set at (0m, 0m) location with a height of 1.8m to 3.0m (0.1m interval) and an inclination angle of 0° to 360° (0.5° interval). The average height of a vehicle was chosen as 1.8m. For 16-laser LiDAR sensors, the size of the study area was defined as [-100m, 100m, -16m, 16m] (considering the shoulder at both sides along Y-axis). For 32-laser LiDAR sensors, the study area was set to [-200m, 200m, -16m, 16m]. In terms of the *MinLaserCount* parameter, we required at least two and four laser beams for 16-laser and 32-laser LiDAR sensors, respectively. If the *MinLaserCount* was set to two or three for 32-laser sensors, the maximal value of the objective function using different installation alternatives was the same. Using the ergodic optimization algorithm, the optimal installation plan (height and inclination) of a single LiDAR sensor is listed in Table 5(a). For example, a Puck LiDAR sensor is horizontally installed at a height of 2.4m as recommended and the corresponding vehicle detection performance in the study area is shown in Fig. 17(a). The vehicles located within the yellow and blue areas can be detected with/without satisfaction of *MinLaserCount* requirement, respectively.

**TABLE 5(a) Installation Recommendation for Single LiDAR Sensor**

| LiDAR Type | Height (m) | Inclination (degree) | Location (m) | MinLaserCount |
|---|---|---|---|---|
| Puck | 2.4 | 0 | (0, 0) | ≥ 2 |
| Puck Hi-Res | 2.1 or 2.2 | 0 | (0, 0) | ≥ 2 |
| Ultra Puck | 1.8 | 0 | (0, 0) | ≥ 4 |

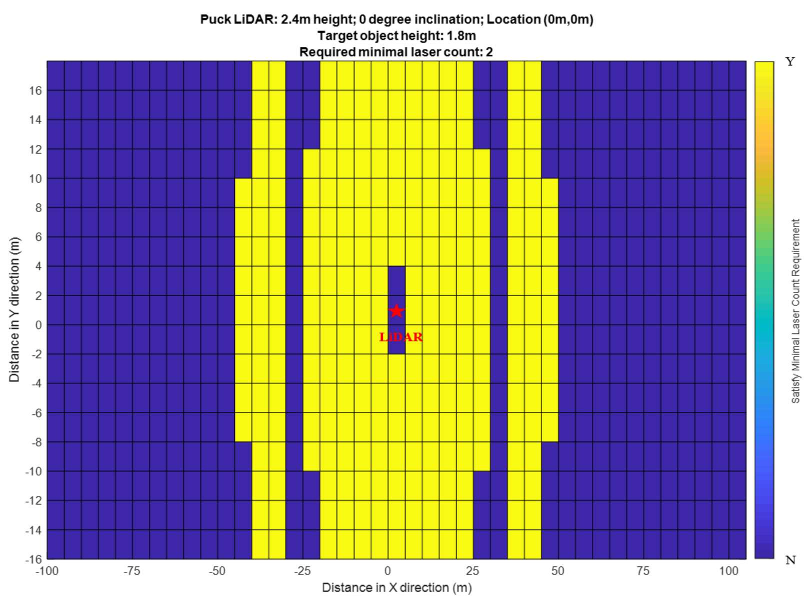


**Fig. 17(a).** Detection performance of single Puck sensor with recommended installation.

For installing multiple LiDAR sensors, a similar optimization problem was defined except that the first constrain was changed to: the total number of valid laser beams from each LiDAR sensor should be greater than or equal to *MinLaserCount.* In our experiment, two 16-laser LiDAR sensors were set at (-75m, 0m) and (75m, 0m) locations and the study area was defined as [-175m, 175m, -16m, 16m]. Two 32-laser LiDAR sensors were set at (-150m, 0m) and (150m, 0m) locations and the study area was [-350m, 350m, -16m, 16m]. The recommendation for multiple sensor installation is listed in Table 5(b). Similar to Fig. 17(a), Fig. 17(b) shows the vehicle detection performance using two Puck LiDAR sensors, which are installed at a height of 2.3m and an inclination of 0.5° in opposite directions. The yellow and blue areas also indicate the regions with/without satisfaction of *MinLaserCount* requirement, respectively.

**TABLE 5(b) Installation Recommendation for Multiple LiDAR Sensors**

| LiDAR Type | Height1 (m) | Inclination1 (degree) | Location1 (m) | Height2 (m) | Inclination2 (degree) | Location2 (m) | MinLaserCount |
|---|---|---|---|---|---|---|---|
| Puck | 2.3 | +0.5 | (–75, 0) | 2.3 | –0.5 | (75, 0) | ≥ 2 |
| Puck Hi-Res | 1.8 | +1.0 | (–75, 0) | 1.8 | –1.0 | (75, 0) | ≥ 2 |
| Ultra Puck | 1.8 | 0 | (–150, 0) | 1.8 | 0 | (150, 0) | ≥ 4 |

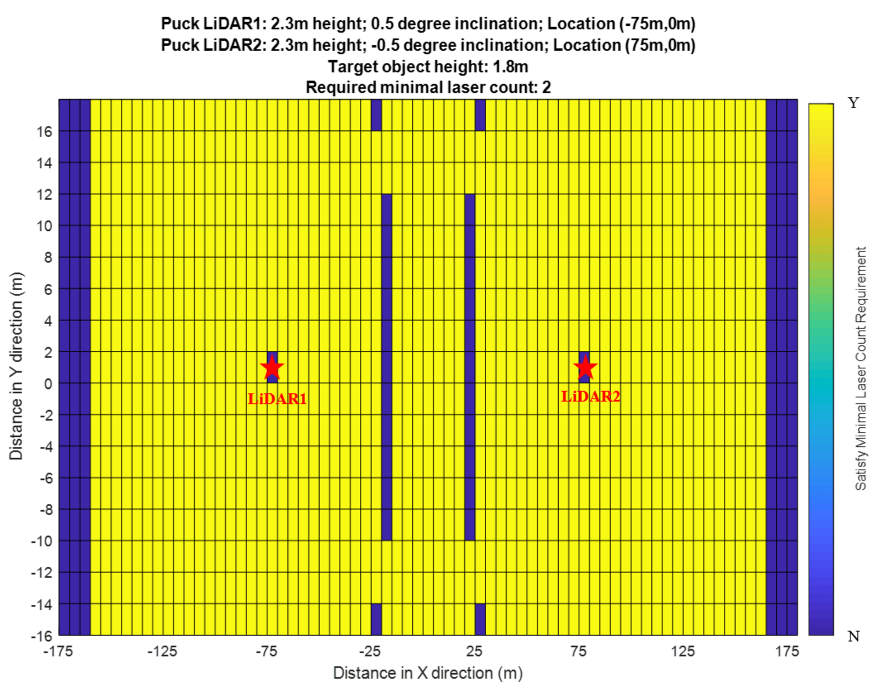


**Fig. 17(b).** Detection performance of multiple Puck sensors with recommended installation.

According to the optimal installation strategies, we found that in terms of two types of 16-laser LiDAR sensors, it is better to deploy Puck Hi-Res sensors at a lower position compared with Puck sensors for detecting target objects within the same study area since the Puck Hi-Res sensor has a smaller vertical FOV (20°) than the Puck sensor (30°). If two sensors of the same height are inclined with the same amount of angle but in opposite directions, the detection performance of target objects within the overlapped area from both sensors can be enhanced. For 32-laser LiDAR sensors, it is recommended to install the sensor at the lowest allowable position horizontally. Two reasons for explaining this conclusion are: 1) 32 laser beams are distributed non-linearly and majority of them are concentrated in the middle range of the vertical FOV; 2) the undetectable area near the LiDAR sensor may get larger if the sensor is installed too high.

## 6. CONCLUSION

To prepare for application of LiDAR sensors to roadside detection of traffic and pedestrians, understanding how installation may affect their performance is critical. This paper analyzed the built-in features of the selected models and conducted both theoretical and experimental studies to explore and examine the installation methods for the best detection range and accuracy. After the theoretical analyses were made, four field test scenarios were developed for examination, in which LiDAR sensors were 1) horizontally installed at different heights; 2) installed at a fixed height with different inclination angles; 3) vertically installed at a fixed height; and 4) horizontally installed at different heights with consideration of occlusion. The examination successfully validated the theoretical study. At last, optimal deployment plans of installing single and multiple LiDAR sensors at a selected road segment were presented in a case study. Besides, although Velodyne products were used in the examination, this study provides general guidance as to how to maximize the performance by using the built-in features of LiDAR sensors.

Given the many advanced features of LiDAR technology, it is foreseeable infrastructure-based LiDAR sensors will soon be deployed to provide real-time and high-resolution trajectory data of all road users to support advanced transportation systems such as connected vehicles and self-driving. Understanding the key factors for installation is no doubt the first step along this path. For future work, the influence of occlusion issues on detection range of multiple LiDAR sensors can be further discussed. Advanced optimization models can be applied to identify optimal LiDAR installation settings in more complex scenarios with considering more comprehensive factors.

## ACKNOWLEDGMENTS

This research was funded by the Nevada Department of Transportation (NDOT) under Grant No. P744-18-803. The authors gratefully acknowledge this financial support.

## REFERENCES

Ahmed, O. S., Franklin, S. E., Wulder, M. A., & White, J. C. (2016). Extending airborne lidar-derived estimates of forest canopy cover and height over large areas using knn with landsat time series data. *IEEE Journal of Selected Topics in Applied Earth Observations and Remote Sensing*, *9*(8), 3489-3496.

Bautista, C. M., Dy, C. A., Mañalac, M. I., Orbe, R. A., & Cordel, M. (2016, May). Convolutional neural network for vehicle detection in low resolution traffic videos. *Proceedings of IEEE Region 10 Symposium (TENSYMP)*, Bali, Indonesia, 277-281.

Cooper, M. A., Raquet, J. F., & Patton, R. (2018). Range Information Characterization of the Hokuyo UST-20LX LIDAR Sensor. *Photonics, 5(2),* 12.

Csanyi, N., & Toth, C. K. (2007). Improvement of lidar data accuracy using lidar-specific ground targets. *Photogrammetric Engineering & Remote Sensing*, *73(4),* 385-396.

Kidono, K., Naito, T., & Miura, J. (2012, September). Reliable pedestrian recognition combining high-definition LiDAR and vision data. *Proceedings of IEEE intelligent transportation systems conference,* Anchorage, AK, 1783-1788.

Klein, L. A. (2017). *ITS Sensors and Architectures for Traffic Management and Connected Vehicles*. CRC Press.

Klein, L. A., Mills, M. K., Gibson, D., & Klein, L. A. (2006). *Traffic detector handbook: Volume II* (No. FHWA-HRT-06-139). United States. Federal Highway Administration.

Kromer, R., Lato, M., Hutchinson, D. J., Gauthier, D., & Edwards, T. (2017). Managing rockfall *Geotechnical Journal*, *54*(7), 953-967.

Lizarazo Jimenez, C. G. (2016). Classification of road users detected and tracked with LiDAR at intersections (Master's thesis). Retrieved from Purdue e-Pubs.

Mahmud, K., Mariethoz, G., Treble, P. C., & Baker, A. (2015). Terrestrial LIDAR survey and morphological analysis to identify infiltration properties in the Tamala Limestone, western Australia. *IEEE Journal of Selected Topics in Applied Earth Observations and Remote Sensing*, *8*(10), 4871-4881.

Mandlburger, G., Hauer, C., Wieser, M., & Pfeifer, N. (2015). Topo-bathymetric LiDAR for monitoring river morphodynamics and instream habitats - A case study at the Pielach River. *Remote Sensing, 7(5),* 6160-6195.

McCoy, P. T., Bonneson, J. A., & Kollbaum, J. A. (1995). Speed reduction effects of speed monitoring displays with radar in work zones on interstate highways. *Transportation Research Record*, *1509*, 65-72.

Premebida, C., Monteiro, G., Nunes, U., & Peixoto, P. (2007, September). A lidar and vision-based approach for pedestrian and vehicle detection and tracking. *Proceedings of IEEE intelligent transportation systems conference*, Seattle, WA, 1044-1049.

Qu, Y., Jiang, L., & Guo, X. (2016). Moving vehicle detection with convolutional networks in UAV videos. *Proceedings of International Conference on Control, Automation and Robotics (ICCAR),* Hong Kong, China, 225-229.

Schubarth, C. (2018). Velodyne halves price on self-driving sensor Zoox, Apple are said to be using. *Silicon Valley Business Journal*. Retrieved from: https://www.bizjournals.com/sanjose/news/2018/01/02/velodyne-lidar-san-jose-price-cut-apple-zoox.html

Velodyne. (2016). VLP-16 Manual: User's Manual and Programming Guide. Velodyne LiDAR. Inc.: San Jose, CA, USA.

Velodyne. (2018). VLP-32C User Manual. Velodyne LiDAR. Inc.: San Jose, CA, USA

Wen, X., Shao, L., Fang, W., & Xue, Y. (2014). Efficient feature selection and classification for vehicle detection. *IEEE Transactions on Circuits and Systems for Video Technology*, *25*(3), 508-517.

Westoby, M. J., Lim, M., Hogg, M., Pound, M. J., Dunlop, L., & Woodward, J. (2018). Cost-effective erosion monitoring of coastal cliffs. *Coastal Engineering*, *138*, 152-164.

Zhao, H., Sha, J., Zhao, Y., Xi, J., Cui, J., Zha, H., & Shibasaki, R. (2012). Detection and tracking of moving objects at intersections using a network of laser scanners. *IEEE transactions on intelligent transportation systems*, *13(2)*, 655-670.

Zhao, H., & Shibasaki, R. (2005). A novel system for tracking pedestrians using multiple single-row laser-range scanners. *IEEE Transactions on systems, man, and cybernetics-Part A: systems and humans*, *35(2)*, 283-291.

Zhao, J., Xu, H., Liu, H., Wu, J., Zheng, Y., & Wu, D. (2019). Detection and tracking of pedestrians and vehicles using roadside LiDAR sensors. *Transportation research part C: emerging technologies*, *100*, 68-87.